Study on the Migration and Transformation of Inorganic Minerals During In-Situ Oil Shale Mining

Qingyu Li
Jilin University
Laijun Lu
Jilin University
Quansheng Zhao
Qingdao University
Shuya Hu (90shuya@qdu.edu.cn)
Qingdao University

Article

Keywords: oil shale in-situ exploitation, groundwater, water-rock interaction, inorganic minerals, hydrogeochemistry

Posted Date: March 17th, 2022

DOI: https://doi.org/10.21203/rs.3.rs-1449231/v1

Abstract

Oil shale has become an important exploration target due to global oil shortages. The process of in-situ exploitation of oil shale requires a large amount of heat, which is bound to destroy the underground environment and make the original tight impervious layer or weak permeable layer become a loose permeable layer, thus affecting groundwater. In this paper, the release of inorganic minerals from oil shale, oil shale ash and surrounding rock to groundwater during in-situ mining has been simulated by laboratory experiments, and its mechanism has been discussed. The results showed that both ambient temperature and reaction time affected the release of anions and cations. Ca^{2+} is the main cation in aqueous solution at 20 ℃ and 50 ℃, and Na^{+} is the main cation in aqueous solution at 80 ℃ and 100 ℃. HCO_3^- is the main anion in the aqueous solution under different reaction conditions. Different from other ions, the content of Ca^{2+}, Mg^{2+}, and HCO_3^- decreased with increasing reaction temperature. With increasing temperature and the progress of the reaction, the water chemical types in the three aqueous solutions change. The hydrochemical type of oil shale ash-aqueous solution changes from HCO_3-Na + K to $SO_4 \cdot HCO_3$-Na + K at 80 ℃ and 100 ℃. The results show that the release of inorganic minerals from oil shale to groundwater cannot be ignored due to the heat released during the in-situ exploitation of oil shale.

Introduction

The reserves of oil on Earth are well known to be limited. According to the data of the remaining proven recoverable oil reserves, updated globally in 2019, the remaining recoverable oil reserves are 230,580,000 tons, which can be exploited for approximately 46.8 years[1]. Therefore, oil shale is an important reserve energy source and has become one of our research foci[2–4]. The global reserves of oil shale are very large, but because oil shale is often interbedded with coal and carbonaceous mudstone, the exploitation of oil shale becomes very difficult, and environmental pollution is one of the difficulties[5–10].To reduce the damage to the environment caused by exploitation, scientists around the world have put forward a variety of methods for the in-situ exploitation of oil shale[11–14]. Compared with traditional surface retorting technology, in situ exploitation does not require mining, transportation or ore processing, in which heat is directly supplied by thermal conduction or thermal radiation to the underground oil shale layer so that the oil shale is cracked underground to generate oil and gas, and then the pyrolysis oil and gas are recovered[15–19].

Under natural conditions, the oil shale layer and upper surrounding rock usually form a dense waterproof layer. However, a large amount of pyrolytic water will be produced during the in situ exploitation of oil shale. In the process of mining, the rock mass ruptures into cracks with increasing thermal stress and release of organic matter[20]. Fracturing and pyrolysis will change the original stress of the overlying rock mass. When the stress exceeds the shear strength of the rock, the rock layer will fracture, resulting in a series of water-conducting fracture zones. The in-situ pyrolysis process causes the oil shale layer to gradually change from the usual water-tight layer or weakly permeable layer to a permeable layer[21–23]. This evolution may lead to a hydraulic connection between the oil shale mining layer and the surrounding aquifer, resulting in different degrees of water-rock interaction between groundwater and oil shale, the ash and slag of oil shale after mining, and the surrounding rock of oil shale[24]. Instead of quickly returning to normal ground temperature after mining, it can take years to cool down, potentially increasing the degree of water-rock interaction and changing the chemistry of the surrounding rock and groundwater.

Regarding the effect of in situ pyrolysis of oil shale on groundwater, a few studies have considered the potential pollution risk of water-rock interaction solutions in oil shale to groundwater, and a series of experimental studies has been carried out. Amy analyzed the organic components leached from in situ pyrolysis waste oil shale by conducting a series of continuous indoor over column leaching experiments, which determined that organic contaminants in the leachate would seriously deteriorate the groundwater quality within the mining area, and it would take decades for the water quality to recover[25]. Wang performed ultrapure water-rock interaction experiments. The results showed that Pb tended to accumulate in solid residues during pyrolysis. The influence of solid residue after pyrolysis of oil shale on the groundwater environment is a continuous process[26]. Hu conducted a series of water-rock interaction experiments between oil shale-water and oil shale ash-water to study the release of organic matter from groundwater during oil shale in situ exploitation. The results showed that the formation of fracture zones promoted by pyrolysis of oil shale will cause organic contaminants to diffuse into deeper groundwater and affect the quality of groundwater[21]. Related studies mainly discuss the impact of organic pollution and heavy metals on the groundwater environment during in situ oil shale mining[27–29], but few previous reports have focused on the impact of inorganic mineral components in the groundwater environment. However, the in-situ exploitation of oil shale is a long process; for example, the in-situ conversion process (ICP) utilizes electricity to heat the oil shale underground needs to continue over 2 years[23]. Studies have shown that oil shale exploitation affects the formation temperature field for a long time, approximately four times the heating time. Therefore, under long-term hydrothermal conditions, the release of inorganic minerals from oil shale to the groundwater environment should not be ignored.

In this study, a series of water-rock interaction experiments including oil shale and water, oil shale ash and water, and surrounding rock and water was conducted. We try to identify the mineral elements of oil shale, oil shale ash, or surrounding rock released into groundwater during the simulated in situ mining process and analyze the potential impact of in situ recovery of oil shale on the aquifer system.

Materials And Methods

Sample and Experiment of Water-rock Interaction. The sampling area is located in the southeast uplift of the Songliao Basin. The oil shale has a grey-brown and dense massive structure with a burial depth of 7-258 m and an oil content of 3.5-5%. Oil shale blocks and the surrounding rock of the upper layer of the oil shale were collected.

The stratified oil shale blocks and surrounding rock of the upper layer of oil shale were crushed and screened to a size range of 2-3cm to obtain experimental samples. The oil shale and surrounding rock were dried in an oven at 110°C for 4 hours before weighing. One-third of the oil shale was heated to 400°C in a tube furnace under nitrogen to obtain oil shale ash samples. Ultrapure water (1L) was added to 100 g oil shale, oil shale ash, and surrounding rock samples.

The samples were placed in water baths with separation temperatures of 20 ± 0.1°C, 50 ± 0.1°C, 80 ± 0.1°C, and 100 ± 0.1°C. Each temperature tank had 10 samples. Samples were soaked for 0.5, 1, 2, 5, 8, 15, 20 and 30 days. After soaking, the aqueous solution sample was filtered and tested.

Cation content determination. The calcium content in the solution was determined by ethylenediaminetetraacetic acid (EDTA) ($C_{10}H_{14}N_2O_8Na_2{\cdot}2H_2O$) titration. The contents of K, Na, and Mg were measured by a Shimadzu AA-6000CF atomic absorption spectrophotometer.

Anion content determination. The content of carbonate and bicarbonate ions in the solution was measured by the acid standard solution titration method (national standard method DZ/T 0064.49–2021). The content of F^-, Cl^-, NO_3^- and SO_4^{2-} in aqueous solution were determined by a Vantone 861 double inhibitory ion chromatograph.

Results And Discussion

Main cation variation characteristics. Figure 1. shows the changes in the main cation content in oil shale-water reaction solutions at different reaction temperatures. The figure shows that under the reaction conditions of 20 °C and 50 °C, the contents of the four cations in the aqueous solution have little difference. At reaction temperatures of 20°C and 50°C, the content of Ca^{2+} is the highest, followed by K^+ and Na^+, and the content of Mg^{2+} is the lowest. At reaction temperatures of 80°C and 100°C, the content of Na^+ in the oil shale-water solution changes strongly; the Na^+ content is the highest, followed by K^+ and Ca^{2+}, and the Mg^{2+} content is the lowest, possibly because Ca^{2+} and Mg^{2+} in aqueous solution come mainly from the dissolution of dolomite and calcite. With increasing temperature, the solubility of dolomite and calcite decreases, and the reaction equations are as follows:

$$CaCO_3 + CO_2 + H_2O \rightarrow Ca^{2+} + 2HCO_3^- \quad (1)$$

$$CaMg(CO_3)_2 + CO_2 + H_2O \rightarrow Ca^{2+} + Mg^{2+} + 4HCO_3^- \quad (2)$$

Moreover, K^+ changes little at 20°C, 50°C, and 80°C but increases rapidly at 100°C, indicating that a temperature of approximately 100°C has the greatest influence on the K^+ content. The cation content in the aqueous solution tends to be stable at approximately 15 days.

As shown in Fig. 2, compared with the cation content in the oil shale-aqueous solution, the cation content in the oil shale ash-aqueous solution shows a different trend with increasing reaction temperature. Under different reaction temperatures, the K^+ content in oil shale ash-aqueous solution always remains the highest, and the K^+ content at 50 °C, 80 °C, and 100 °C is twice the K^+ content at 20 °C. At 20°C, the average content of Na^+ (5.79 mg/L) was lower than the average content of Ca^{2+} (7.10 mg/L), but with increasing reaction temperature, the Na^+ content gradually increased and remained higher than the Ca^{2+} content. Ca^{2+} has a declining trend with increasing temperature. Under a reaction temperature of 100°C, the Na^+ content in the oil shale ash-aqueous solution increases rapidly with increasing reaction time. After 30 days of reaction, the Na^+ content reached 16.10 mg/L, which was close to the K^+ content, indicating that high temperature is favorable for the dissolution of Na and K minerals in oil shale ash.

The variation in the content of the main cations in the surrounding rock-aqueous solution with different reaction temperatures is shown in Fig. 3. With increasing reaction time, the content of cations showed an upwards trend. Under the reaction conditions of 20°C and 50°C, the content of Ca^{2+} in the aqueous solution was the highest, followed by Na^+ and K^+, and Mg^{2+} was the lowest. The content of Na^+ is the highest at 80°C and 100°C, followed by Ca^{2+}, K^+, and Mg^{2+}. With increasing reaction time, the cationic content in aqueous solution increased steadily under the reaction condition of 80°C but fluctuated greatly under the reaction condition of 100°C.

Main anion variation characteristics. The variation trend of the major anion content in the oil shale-aqueous solution under different temperature reaction conditions is shown in Fig. 4. The content of HCO_3^- is always the highest, followed by Cl^-, and the content of HCO_3^- is more than 15 mg/L in the aqueous solutions at different reaction temperatures. When the reaction temperature was 20 °C, 50 °C and 100 °C, the content of Cl^- increased significantly with increasing reaction time, especially when the reaction temperature was 100 °C. After 30 days of reaction, the content of Cl^- reached 15.4 mg/L. The content change of SO_4^{2-} is similar to the content change of Cl^-, and the change is small at reaction temperatures of 20°C, 50°C, and 80°C. The content of SO_4^{2-} in aqueous solution is less than 3 mg/L, but the content of SO_4^{2-} increases sharply at a reaction temperature of 100°C. The content of F^- and NO_3^- in the aqueous solution are always low at different temperature gradients.

The variation in the main anion content in oil shale ash slag-aqueous solution with reaction temperature is shown in Fig. 5. HCO_3^- is the main anion in aqueous solution, the content of HCO_3^- is greater than the content of oil shale aqueous solution, and the content is more than 20 mg/L. The content of HCO_3^- decreases with increasing reaction time in aqueous solutions with higher reaction temperatures (80 °C and 100 °C). Different from oil shale aqueous solution, the content of SO_4^{2-} in aqueous solution increases significantly, and SO_4^{2-} becomes the second-largest anion, surpassing the content of Cl^-. With increasing reaction time, the content of SO_4^{2-} also increases, especially after 30 days of reaction at 80°C, and the content of SO_4^{2-} in aqueous solution reaches 36.97 mg/L. SO_4^{2-} in aqueous solution generally comes from the dissolution of minerals containing gypsum or other sulfates. In addition, oil shale and its surrounding rock contain a large amount of pyrite. Oxidation of pyrite results in the presence of water-insoluble sulfur in water as SO_4^{2-}. At 100°C water temperature, the growth rule of Cl^- is similar to that of SO_4^{2-}. The F^- and NO_3^- content is still low, and the NO_3^- content is almost zero.

Figure 6. describes the changes in the main anion content in the surrounding rock-aqueous solution at different reaction temperatures. Under the reaction conditions of 20 °C, 50 °C, and 80 °C, the variation trend of the main anions in the oil shale surrounding rock water solution is similar to the variation trend of the main anions in the oil shale water solution. HCO_3^- is the main anion, followed by Cl^-, and the content of HCO_3^- and Cl^- gradually increases with time. However, at the reaction temperature of 100°C, HCO_3^- and Cl^- content changes differently from other temperature conditions, and both of these ions increase

first and then decrease with the reaction time. The content of SO_4^{2-}, F- and NO_3^- in the aqueous solution did not change significantly and remained at a low level.

Analysis of migration mechanism. The correlation coefficient can accurately describe the degree of correlation between variables in numerical form[30]. The correlation coefficient matrix can reflect the correlation between each research parameter and characterize the coexistence of the whole dataset or the relationship between any two indices[31]. The Pearson correlation coefficient matrix of each hydrogeochemical index was calculated by SPSS software, as shown in Table 1.

Table 1
The Pearson correlation coefficient matrix

	K	Na	Mg	Ca	HCO_{3-}	F	Cl	NO_3	SO_4	pH	conductivity	reaction time	reaction tempera
K	1.000	**0.731****	-0.204*	0.290**	**0.821****	0.029	0.451**	-0.272**	**0.857****	0.355**	**0.765****	0.078	0.310**
Na		1.000	-0.341**	0.240*	**0.674****	0.254**	**0.796****	-0.406**	**0.697****	0.159	**0.859****	0.420**	**0.576****
Mg			1.000	0.472**	0.068	-0.248**	-0.218*	0.076	-0.129	-0.011	-0.165	0.129	**-0.639****
Ca				1.000	**0.688****	-0.193*	0.149	-0.210*	0.239*	0.130	0.340**	0.204*	-0.186
HCO_3-					1.000	-0.046	0.342**	-0.359**	**0.612****	0.329**	**0.678****	0.131	0.186
F						1.000	0.291**	0.087	-0.027	0.116	0.188	0.143	0.338**
Cl							1.000	-0.334**	**0.509****	-0.067	**0.672****	**0.506****	0.491**
NO_3								1.000	– .277**	0.126	– .368**	-0.103	-0.335**
SO_4									1.000	0.200*	**0.790****	0.206*	0.227*
pH										1.000	0.240*	-0.079	0.017
conductivity											1.000	0.287**	0.424**
reaction time												1.000	0.000
reaction temperature													1.000
lithology													
*represents a significant correlation at the 0.01 level (bilateral).													
** represents a significant correlation at the 0.05 level (bilateral).													

According to the correlation coefficient matrix, lithology has a great influence on K^+, HCO_3^-, and SO_4^{2-} content and electrical conductivity in the water-rock interaction, showing a strong positive correlation.

The reaction time was positively correlated with Cl^- content. In the aqueous solution, Cl^- comes mainly from the dissolution of rock salt (NaCl) or other chlorides ($MgCl_2$, $CaCl_2$). Chlorine salts are highly soluble and do not easily precipitate from water. The reaction temperature has a great influence on the content of Na^+ and Mg^{2+}. With increasing reaction temperature, the Na^+ content increases, while the Mg^{2+} content shows the opposite trend. Ca^{2+} and Mg^{2+} in aqueous solution come mainly from the dissolution of dolomite and calcite. The solubility of dolomite and calcite decreases with increasing temperature. Although the reaction temperature is negatively correlated with Ca^{2+}, the correlation is not strong, indicating that there are other factors affecting the Ca^{2+} content in the aqueous solution.

There is a strong positive correlation between Ca^{2+} and HCO_3^- in the aqueous solution because carbon dioxide in an aqueous solution will increase the solubility of $CaCO_3$. The content of HCO_3^- depends on the partial pressure of CO_2 in aqueous solution. Figure 7. depicts the ionic ratio relationship between Ca^{2+} and HCO_3^-. The results showed that only one water sample point was between 1:1 and 1:2, and the mole ratios of Ca^{2+} and HCO_3^- in other reaction solutions were all below the 1:2 line, indicating that calcite in aqueous solution may dissolve faster than dolomite, and calcite reaches supersaturation earlier than dolomite and precipitates calcite. The dissolution of dolomite also reacts with CO_2 in an aqueous solution to produce HCO_3^-, making the mole ratios of Ca^{2+}, Mg^{2+}, and HCO_3^- between 1:1 and 1:2. $^+$ in aqueous solution.

The ratio relationship between Ca^{2+}, Mg^{2+}, and HCO_3^- is shown in Fig. 8. In the water-rock interaction solution, only part of the samples are between 1:1 and 1:2 under the reaction condition of 20 °C, and most of the sample points are below the ratio of 1:2, suggesting that solutions of dolomite and calcite are only

part of the source of HCO_3^-. In addition, the solubility of Na_2CO_3 is very high. When the concentration of Na^+ in an aqueous solution is high, the content of HCO_3^- will exceed the upper limit related to Ca^{2+}.

K^+ was positively correlated with Na^+, HCO_3^- and SO_4^{2-}, Na^+ was positively correlated with Cl^-, and HCO_3^- was positively correlated with SO_4^{2-}, suggesting that they have the same material source or formation. The K^+ in aqueous solution comes mainly from the dissolved K^+ of illite:

$$K_{0.5}Mg_{0.25}Al_{2.3}Si_{3.5}O_{10}(OH)_2 + 11/10H^+ + 63/20H_2O \rightarrow 23/20Al_2Si_2O_5 + 1/2K + 1/4Mg^{2+} + 6/5Si(OH)_4 \quad (3)$$

Figure 9. shows the scattering of γNa/γCl in the aqueous solution under different reaction conditions. The results show that most of the points fall below the 1:1 line. The content of Na^+ in the aqueous solution is higher than the content of Cl^-, especially in the aqueous solution with a higher reaction temperature, indicating that rock salt is not the only source of sodium ions in aqueous solution, and sodium ions also come from the dissolution of plagioclase and sodium montmorillonite. An increase in reaction temperature will promote the dissolution of these minerals:

$$NaAlSi_3O_8 + H^+ + 9/2H_2O \rightarrow 1/2Al_2Si_2O_5(OH)_4 + Na^+ + Si(OH)_4 \quad (4)$$

$$3Na_{1/3}Al_{7/3}Si_{11/3}O_{10} + 30H_2O + 6OH^- \rightarrow Na^+ + 7Al(OH)_4^- + 10H_4SiO_4 \quad (5)$$

SO_4^{2-} in solution usually comes from the dissolution of gypsum or other sulfates. In addition, the oxidation of pyrite in oil shale and surrounding rock leads to the existence of water-insoluble sulfur in water in the form of SO_4^{2-}.

$$2FeS_2 + 7O_2 + 2H_2O + 2FeSO_4 + 4H^+ + 2SO_4^{2-} \quad (6)$$

Fluorine comes mainly from the hydrolysis of fluorite (CaF_2) and apatite ($Ca_5(Cl,F,OH)(PO_4)_3$). F^- in aqueous solution can react with Ca^{2+} to form CaF_2. The solubility product of CaF_2 is $10^{-10.4}$. Therefore, the Ca^{2+} concentration is an important factor in controlling the F^- content in aqueous solutions.

Analysis of the characteristics of water chemical evolution. The Piper diagram can reflect the chemical composition of water-rock interactions in aqueous solution, as shown by the Piper diagrams of different types of aqueous solutions (Fig. 10). With the progress of the reaction, the hydrochemical type of oil shale water melts gradually and changes from HCO_3-Ca type to HCO_3·Cl-Ca·Na type at 20 °C and 50 °C and from HCO_3-Ca·Na type to HCO_3-Na·Ca type at 80 °C and at 100 °C, HCO_3-Na·Ca type to HCO_3·Cl-Na type. The hydrochemical types of oil shale ash aqueous solution transition from HCO_3·SO_4-Ca type to HCO_3-Ca·Na type at 20 °C, from HCO_3-Ca·Na + K type to HCO_3-Na + K·Ca type at 50 °C, and from HCO_3-Na + K type to SO_4·HCO_3-Na + K type at 80 °C and 100 °C. At 20 °C, the hydrochemical type of oil shale surrounding rock solution transitions from HCO_3-Ca type to HCO_3·Cl-Ca·Na type and remains HCO_3-Ca·Na type at 50 °C. At 80 °C and 100 °C, the solution transitions from the HCO_3·Cl-Ca·Na type and HCO_3-Na·Ca type to the HCO_3·Cl-Na·Ca type, respectively.

With increasing temperature and the progress of the reaction, the content of Ca^{2+}, Mg^{2+} and HCO_3^- in aqueous solution gradually decreases, while the content of Na^+ and K^+ increases. The content of SO_4^{2-} in different aqueous solutions is obviously different. The content of SO_4^{2-} in the oil shale water solution is the highest, followed by the oil shale water solution, and the content of SO_4^{2-} in the oil shale surrounding rock water solution is the lowest.

Analysis of mineral saturation index change. The chemical composition of an aqueous solution is affected mainly by mineral dissolution and precipitation in the process of water-rock interaction. The saturation index (SI) is a commonly used index to judge the saturation of mineral components in solution. Figure 11. shows the variation in the saturation indices of calcite, stone salt, dolomite, gypsum, and fluorite with total dissolved solids (TDS) in water-rock interaction aqueous solutions.

As the figure shows, the saturation index of calcite, salt, dolomite, gypsum and fluorite in each aqueous solution is less than zero, indicating that these minerals are unsaturated in the aqueous reaction solution and can continue to dissolve. In the aqueous solutions of different reaction substances, except for dolomite, the saturation index of other minerals shows little change, presenting a rising trend with the increase in TDS of aqueous solutions and is closer to 0.

Conclusion

Under the conditions of 20 °C and 50 °C, the Ca^{2+} content in the aqueous solution is the highest. Under the conditions of 80°C and 100°C reactions, the content of Na^+ and K^+ in the aqueous solution increased obviously, and Na^+ becomes the main cation. HCO_3^- is the main anion in the aqueous solution under different reaction conditions. Different from other ions, the content of Ca^{2+}, Mg^{2+}, and HCO_3^- decreases with increasing reaction temperature. Lithology has a strong positive correlation with K^+, HCO_3^- and SO_4^{2-} content and conductivity of the aqueous solution. With increasing temperature and the progress of the reaction, the hydrochemical types in the three aqueous solutions all change. The content of SO_4^{2-} in the oil shale ash slag-aqueous solution is high, and the hydrochemical type of the aqueous solution changes from HCO_3-Na + K to SO_4·HCO_3-Na + K at 80 °C and 100 °C.

Declarations

Acknowledgements

We are grateful for the help from the staff of Jilin University and Qingdao University.

Author contributions

Q.L. and S.H. processed the data and analysed the results; Q.L. wrote the manuscript; L.L. drew the figures; L.L. and Q.Z. reviewed the manuscript and made helpful suggestions.

Funding

This work was supported by the National Natural Science Foundation of China (Grant No. 42002260).

Competing interests

The authors declare no competing interests.

References

1. 1Li BL. (2017) China petroleum & chemical corporation, [J].(2):1.
2. Zhang P, Lu S, Li J, Zhang J, Xue H, Chen C. (2017) Comparisons of SEM, Low-Field NMR, and Mercury Intrusion Capillary Pressure in Characterization of the Pore Size Distribution of Lacustrine Shale: A Case Study on the Dongying Depression, Bohai Bay Basin, China. Energy & Fuels 31(9), 9232–9239. https://doi.org/10.1021/acs.energyfuels.7b01625
3. Hu S, Xiao C, Jiang X, Liang X. (2018) Potential Impact of In-Situ Oil Shale Exploitation on Aquifer System. Water 10(5), 649. https://doi.org/10.3390/w10050649
4. Jaber JO, Probert SD. (1999) Environmental-impact assessment for the proposed oil-shale integrated tri-generation plant[J]. Applied Energy, 62(3):169–209. https://doi.org/10.1016/s0306-2619(99)00006-9
5. Altun NE, Hicyilmaz C, Wang JY, Baggi AS, Kok, MV. (2006) Oil shales in the world and Turkey; reserves, current situation and future prospects: a review, Oil Shale 23 211–227.
6. Kok MV. (2006) Oil shale resources in Turkey, Oil Shale 23 209–210.
7. Taciuk W. (2013) Does oil shale have a significant future? Oil Shale 30 1–5. https://doi.org/10.3176/oil.2013.1.01
8. Wang S, Jiang X, Han X, Tong J. (2012) Investigation of Chinese oil shale resources comprehensive utilization performance. Energy 42(1), 224–232. https://doi.org/10.1016/j.energy.2012.03.066
9. Jiang X, Han X, Cui Z. (2007) New technology for the comprehensive utilization of Chinese oil shale resources. Energy 32(5), 772–777. https://doi.org/10.1016/j.energy.2006.05.001
10. Han X, Niu M, Jiang X. (2014) Combined fluidized bed retorting and circulating fluidized bed combustion system of oil shale: 2. Energy and economic analysis. Energy 74, 788–794. https://doi.org/10.1016/j.energy.2014.07.050
11. Gross SA, Avens HJ, Banducci AM, Sahmel J, Panko JM, Tvermoes BE. (2013) Analysis of BTEX groundwater concentrations from surface spills associated with hydraulic fracturing operations. J Air Waste Manag Assoc 63(4), 424–432. https://doi.org/10.1080/10962247.2012.759166
12. Arthur MA, Cole DR. (2014) Unconventional Hydrocarbon Resources: Prospects and Problems. Elements 10(4), 257–264. https://doi.org/10.2113/gselements.10.4.257
13. Jefimova J, Irha N, Reinik J, Kirso U, Steinnes E. (2014) Leaching of polycyclic aromatic hydrocarbons from oil shale processing waste deposit: a long-term field study. Sci Total Environ 481, 605–610.https://doi.org/10.1016/j.scitotenv.2014.02.105 (2014).
14. Jefimova J, Kirso U, Urb G, Steinnes E, Reinik J, Irha N. (2013) Leachability of Trace Elements from the Aged and Fresh Spent Shale Deposit – a Field Study. Oil Shale 30(3), 456. https://doi.org/10.3176/oil.2013.3.06 (2013).
15. Pan Y, Zhang XM, Liu SH, Yang SC, Ren N.(2012) A review on technologies for oil shale surface retort. Chem Soc Pak 34 (6)1331–1338.
16. Qian JL, Yin L. (2011) Oil Shale-supplementary Energy of Petroleum, 1st ed., Beijing: China Petrochemical Press, Chinese.
17. Gavrilova O, Vilu R, Vallner L. (2010) A life cycle environmental impact assessment of oil shale produced and consumed in Estonia. Resources, Conservation and Recycling 55(2), 232–245.https://doi.org/10.1016/j.resconrec.2010.09.013
18. Velts O, Uibu M, Rudjak I, Kallas J, Kuusik R. (2009) Utilization of oil shale ash to prepare PCC: Leachibility dynamics and equilibrium in the ash-water system. Energy Procedia 1(1), 4843–4850. https://doi.org/10.1016/j.egypro.2009.02.312
19. Trikkel A, Kuusik R, Martins A, Pihu T, Stencel J.M. (2008) Utilization of Estonian oil shale semicoke. Fuel Processing Technology 89(8), 756–763.https://doi.org/10.1016/j.fuproc.2008.01.010
20. Yu F, Sun P, Zhao K.a, Ma L, Tian X. (2020) Experimental constraints on the evolution of organic matter in oil shales during heating: Implications for enhanced in situ oil recovery from oil shales. Fuel 261, 116412. https://doi.org/10.1016/j.fuel.2019.116412
21. Hu S, Wu H, Liang X, Xiao C, Zhao Q, Cao Y, Han X. (2022) A preliminary study on the eco-environmental geological issue of in-situ oil shale mining by a physical model. Chemosphere 287(Pt 1), 131987. https://doi.org/10.1016/j.chemosphere.2021.131987
22. Hu S, Xiao C, Liang X, Cao Y, Wang, X, Li M. (2019) The influence of oil shale in situ mining on groundwater environment: A water-rock interaction study. Chemosphere 228, 384–389.https://doi.org/10.1016/j.chemosphere.2019.04.142
23. Brandt AR. (2008) Converting oil shale to liquid fuels: energy inputs and greenhouse gas emissions of the shell in situ conversion process. Environmental Science & Technology, 42(19), 7489–7495. https://doi.org/10.1021/es800531f

24. Hu S, Xiao C, Liang X, Cao Y. (2020). Influence of water-rock interaction on the ph and heavy metals content of groundwater during in-situ oil shale exploitation. Oil Shale, 37(2), 104.https://doi.org/10.3176/oil.2020.2.02
25. Amy GL. (1978) Contamination of groundwater by organic pollutants leached from in-situ spent shale[J]. Office of Scientific & Technical Information Technical Reports, 3. https://doi.org/10.2172/1064003
26. Wang H, Zhang W, Qiu S, Liang X. (2021) Release characteristics of Pb and BETX from in situ oil shale transformation on groundwater environment. Sci Rep 11(1), 16166.https://doi.org/10.1038/s41598-021-95509-2
27. Erg K. (2006) Changes in groundwater sulphate content in estonian oil shale mining area. Oil Shale, 22(3), 275–289.
28. Arthur MA, Cole DR. (2014) Unconventional Hydrocarbon Resources: Prospects and Problems. Elements 10(4), 257–264. https://doi.org/10.2113/gselements.10.4.257
29. Perens R, Punning J M, Reinsalu E. (2006) Water problems connected with oil shale mining in North-East Estonia[J]. Oil Shale23(3):228–235.
30. Li C, Mao J, Liu Q. Application of MODIS satellite remote sensing aerosol products in the study of Air pollution in Beijing [J]. Science in China series D, 2005, 35(A01):10.
31. Li P, Wu J, Qian H. Influences of the model initial value of Holt exponential smoothing model on the water quality prediction accuracy[J]. Geotechnical Investigation & Surveying, 2014(1):4.

Figures

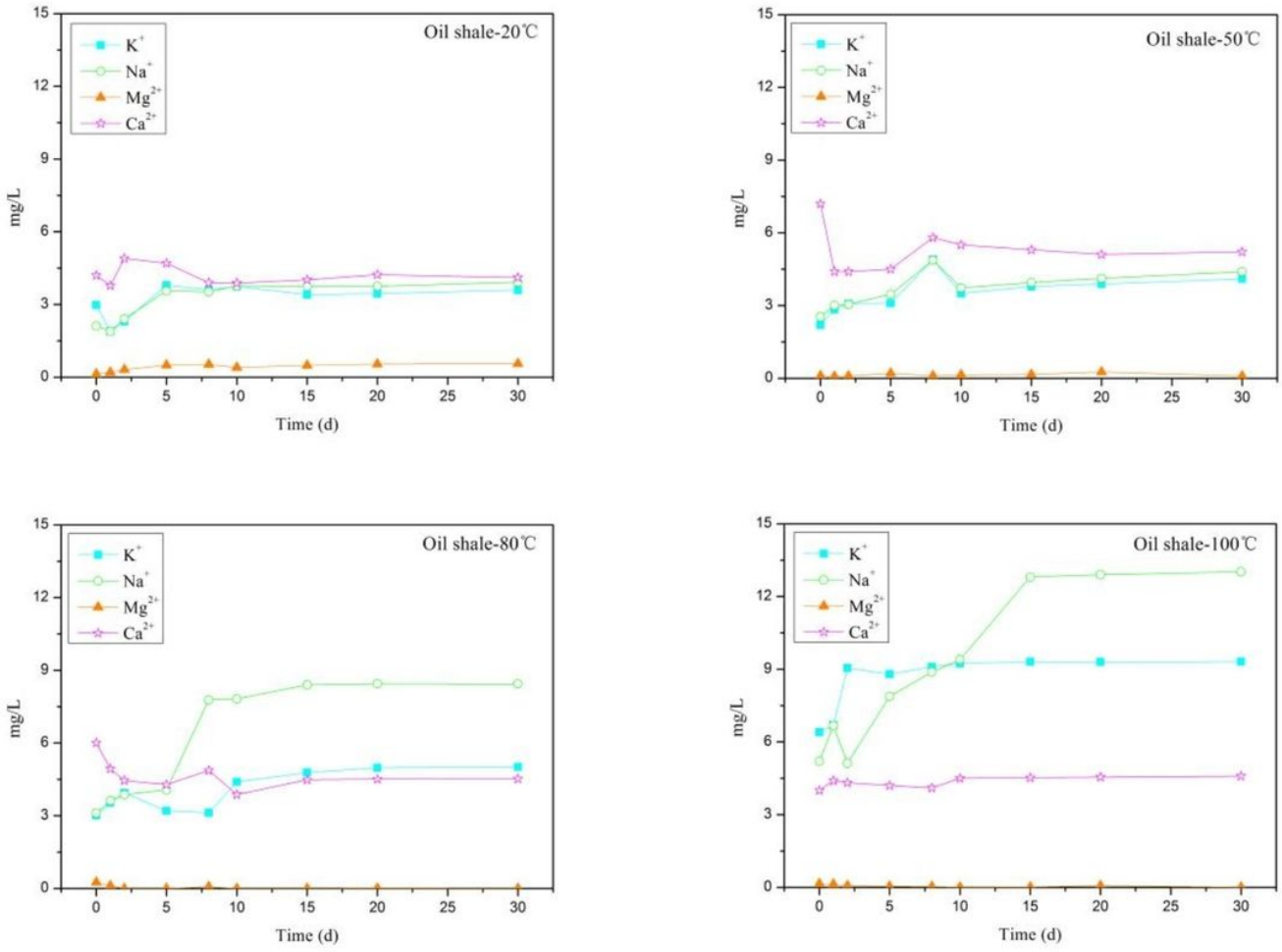

Figure 1

Variations in the content of the main cations in oil shale-aqueous solution under different temperature reaction conditions

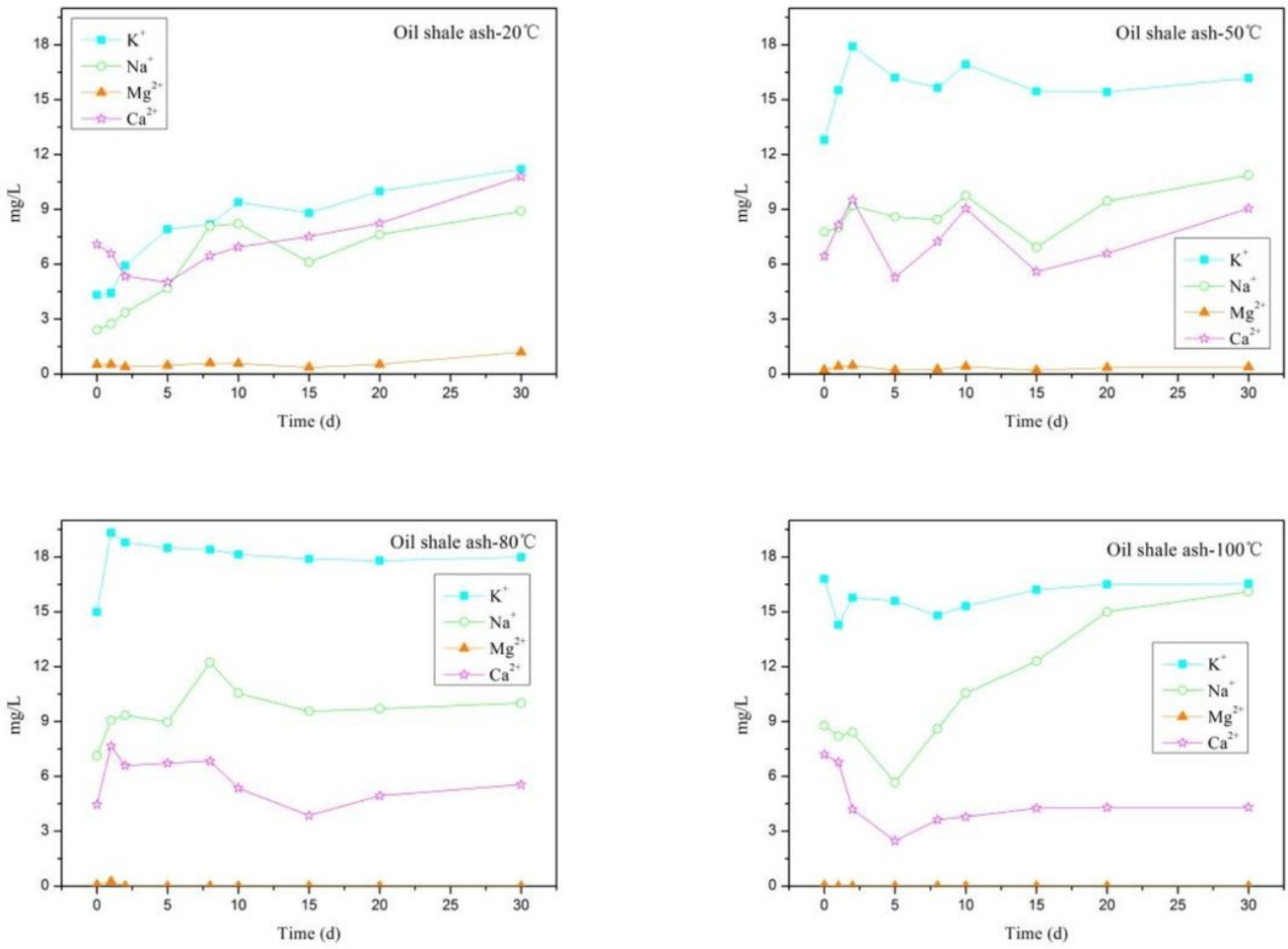

Figure 2

Variation in the content of the main cations in oil shale ash-aqueous solution under different temperature reaction conditions

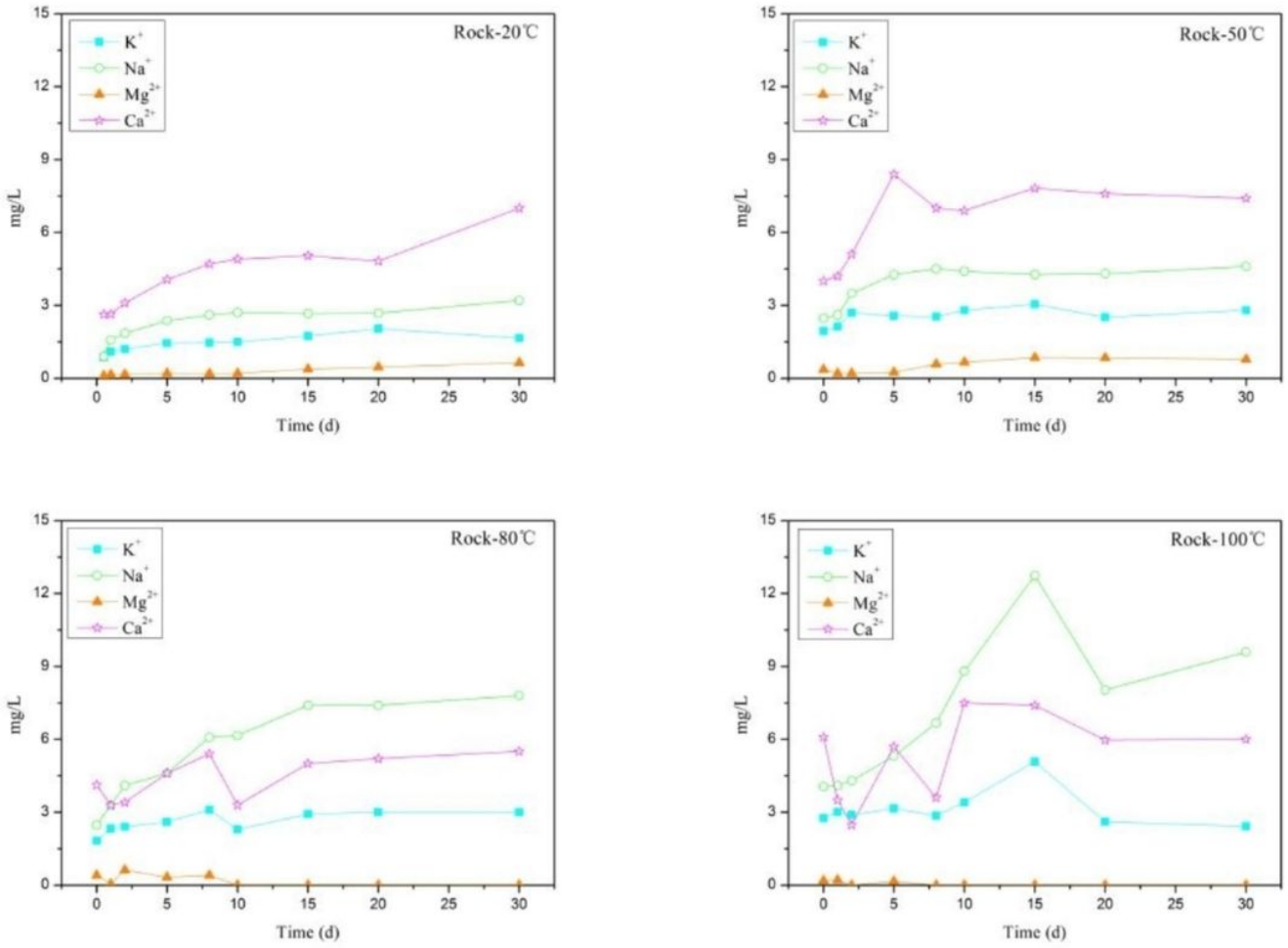

Figure 3

Variation in the content of the main cations in the oil shale surrounding rock-aqueous solution under different temperature reaction conditions

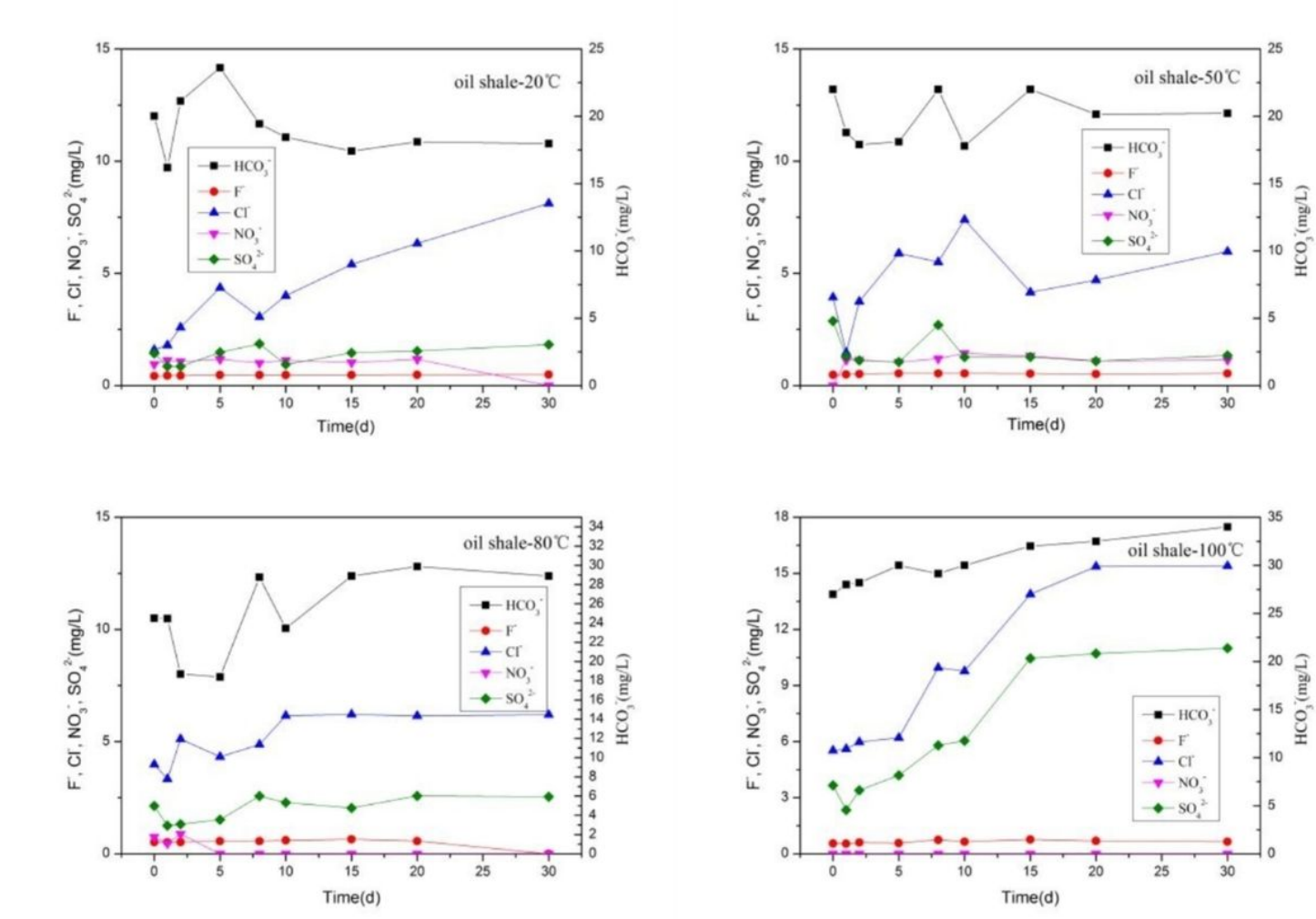

Figure 4

Variation in the content of the main anions in oil shale-aqueous solution under different temperature reaction conditions

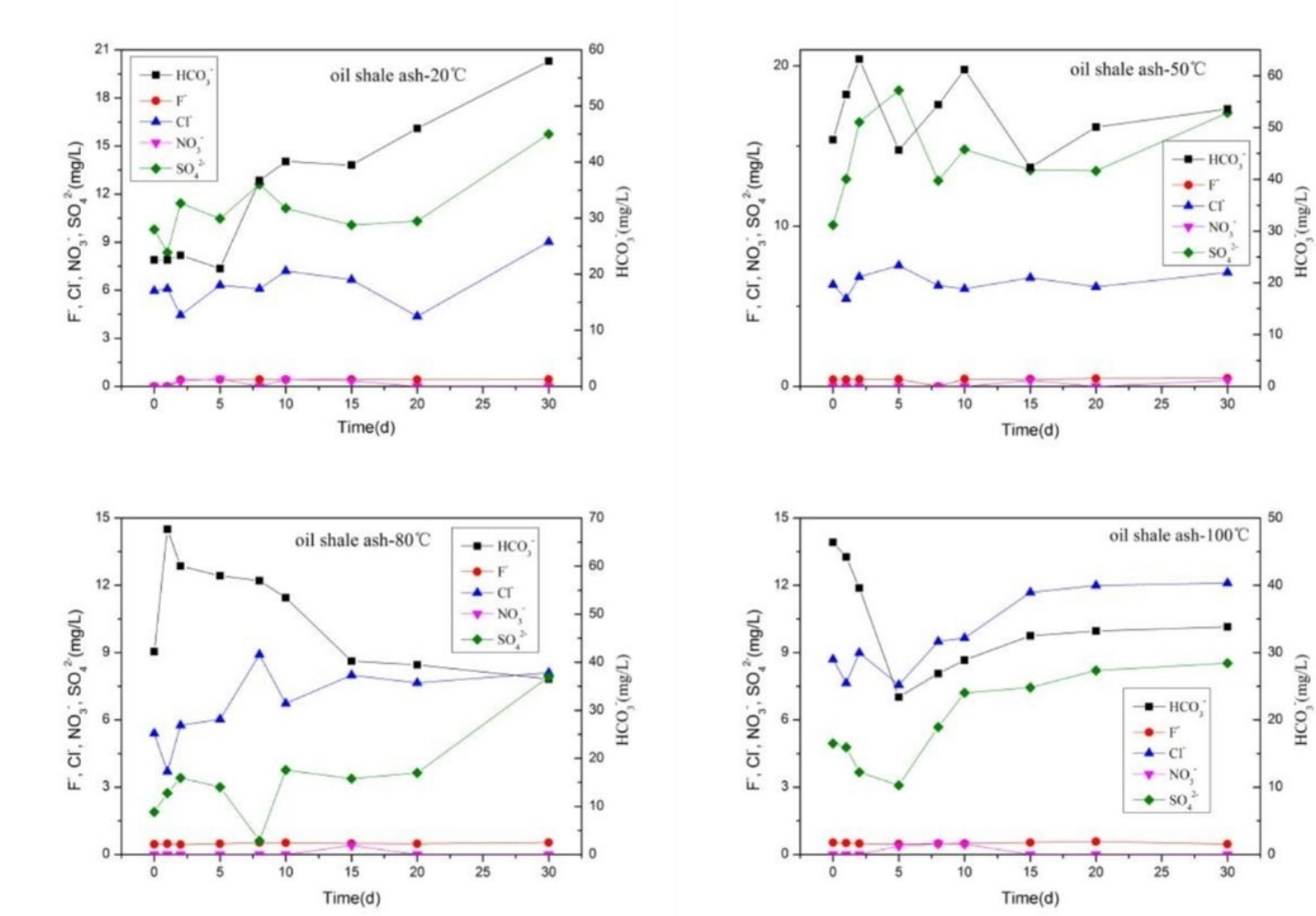

Figure 5

Variation in the content of the main anions in oil shale ash-aqueous solution under different temperature reaction conditions

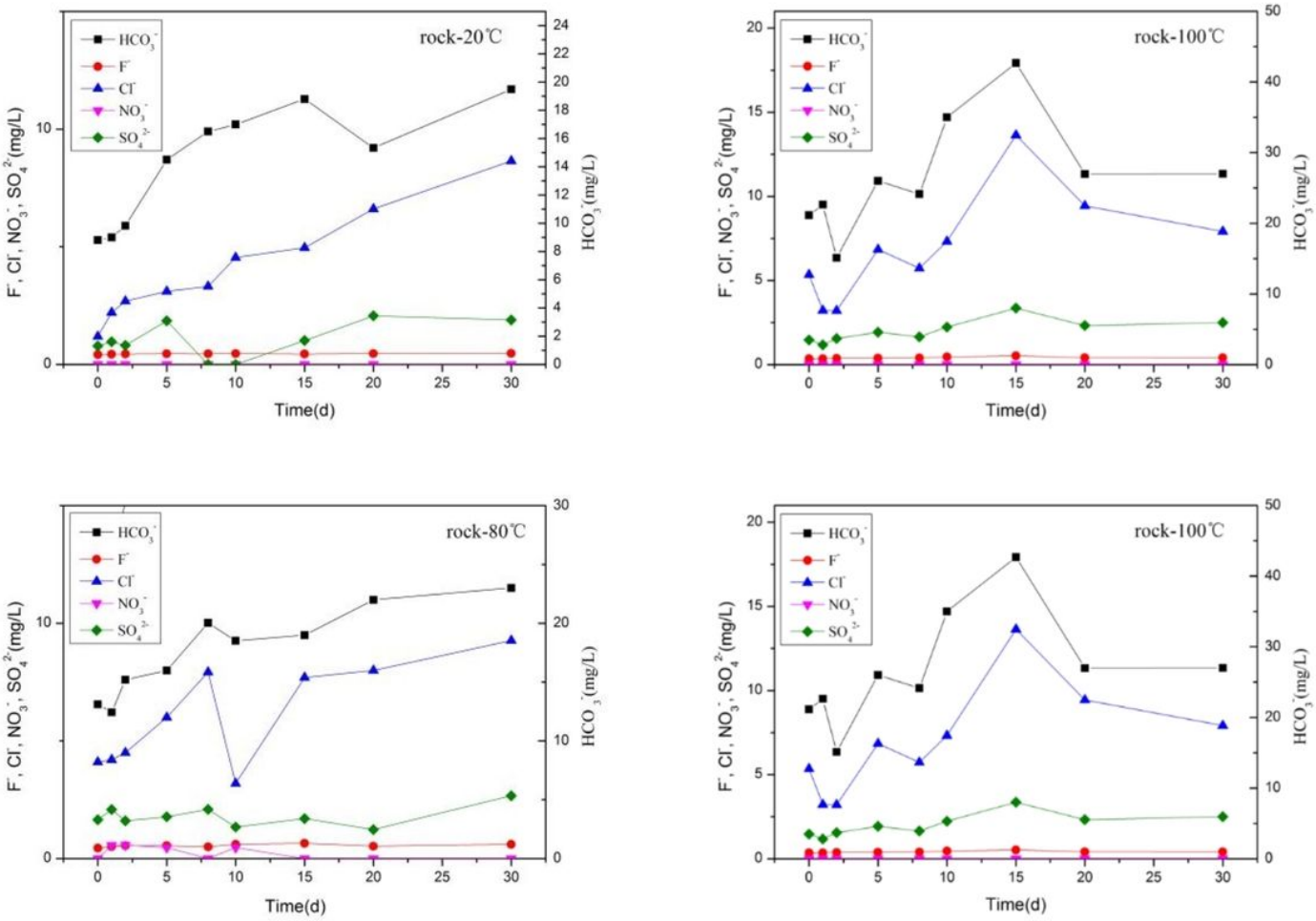

Figure 6

Variation in the content of the main anions in the surrounding rock-aqueous solution under different temperature reaction conditions

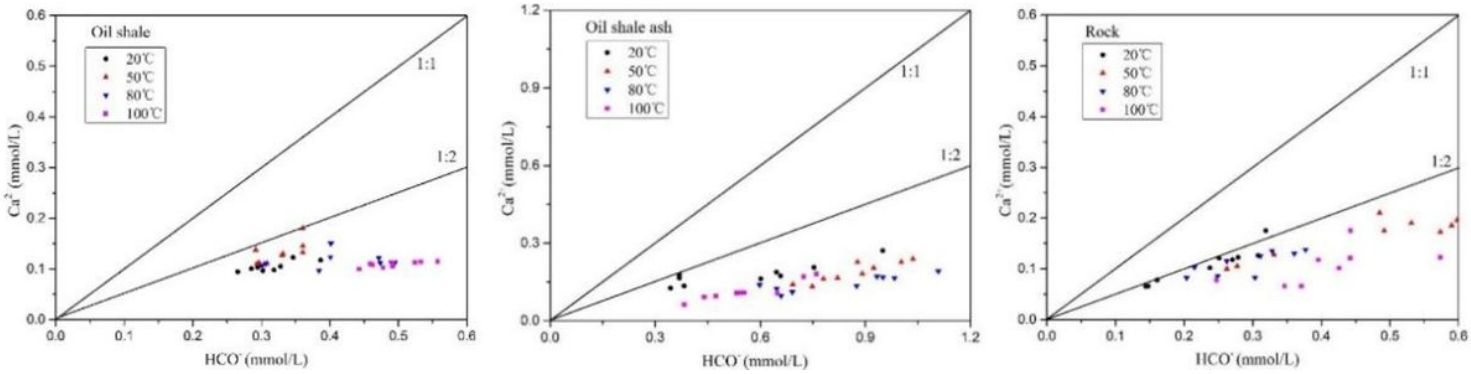

Figure 7

The ratio of Ca^{2+} and HCO_3^- in aqueous solution under different reaction conditions

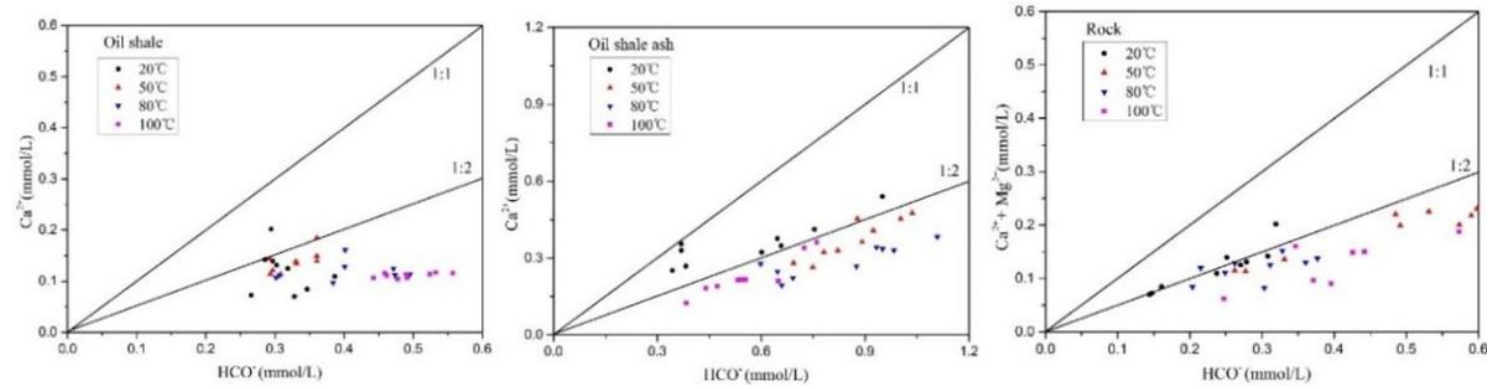

Figure 8

The ratio of Ca^{2+}, Mg^{2+}, and HCO_3^- in aqueous solution under different reaction conditions

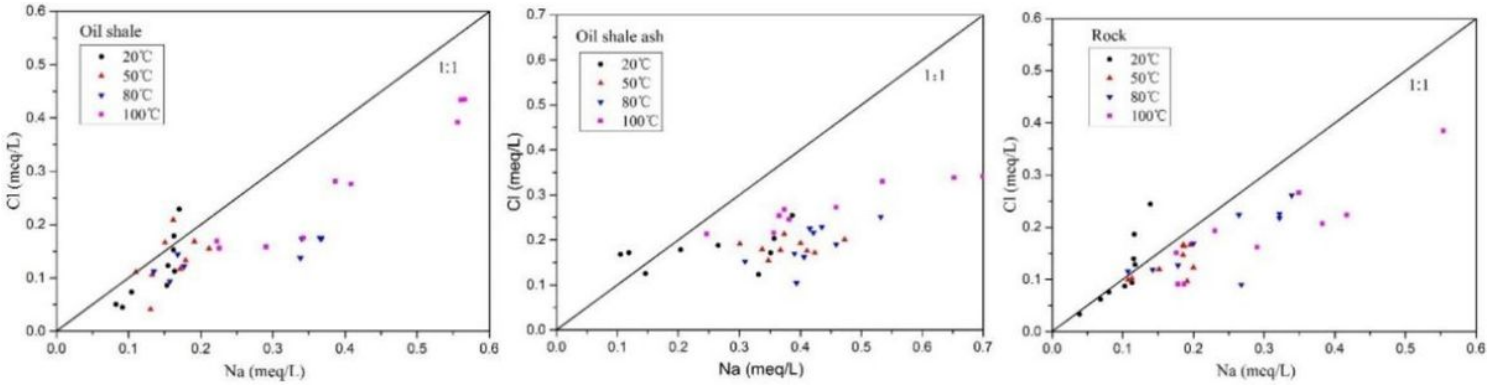

Figure 9

Scatter diagram of γNa/γCl in aqueous solution under different reaction conditions

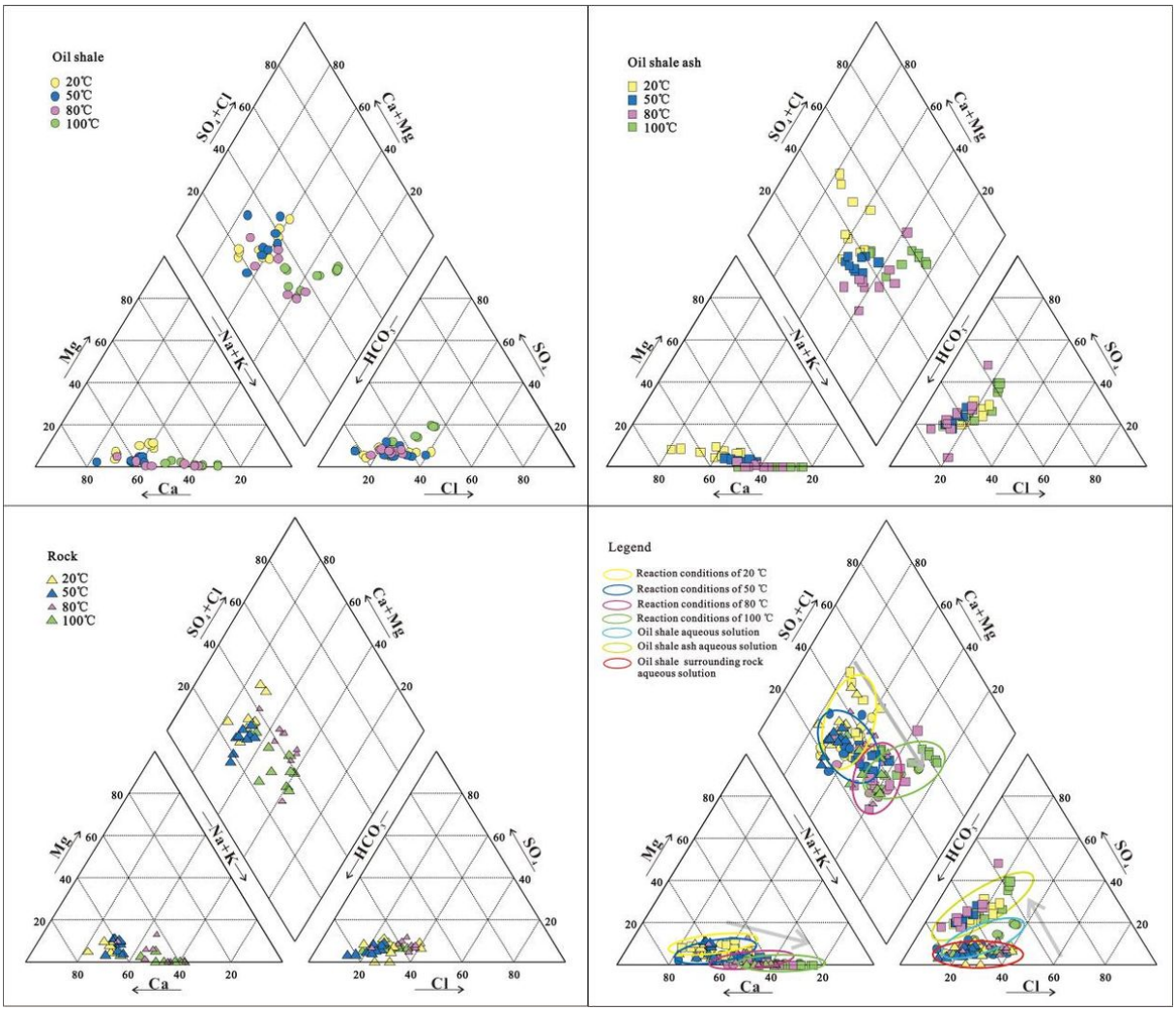

Figure 10

Piper ternary diagram of water-rock interaction aqueous solution with different reaction conditions

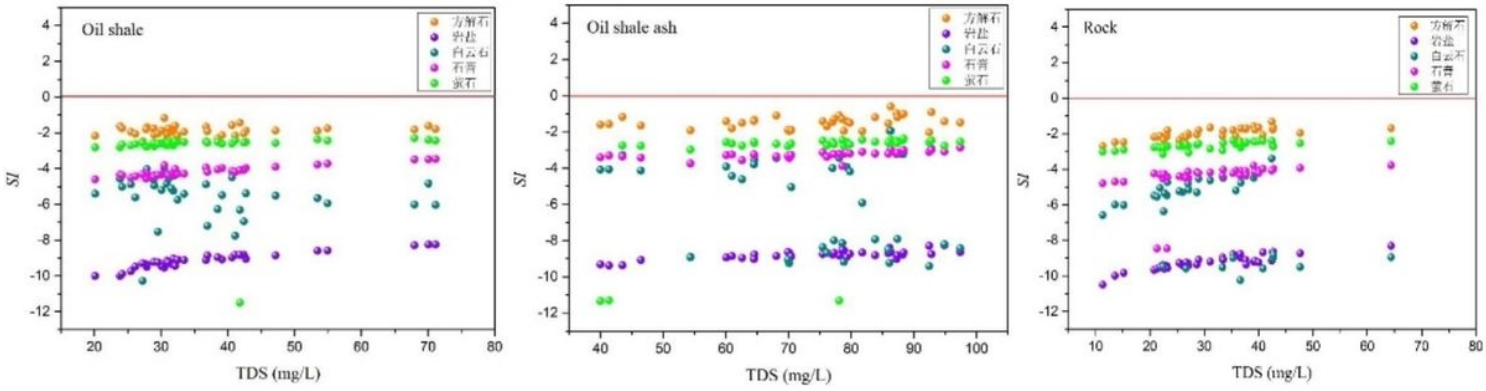

Figure 11

Saturation index of major minerals in aqueous solution with water-rock interactions